

CHUTE DESIGN CONSIDERATIONS FOR FEEDING AND TRANSFER

A.W. Roberts

Emeritus Professor and Director.
Centre for Bulk Solids and Particulate Technologies,
University of Newcastle, NSW, Australia.

SUMMARY

Chutes used in bulk handling operations are called upon to perform a variety of operations. For instance, accelerating chutes are employed to feed bulk materials from slow moving belt or apron feeders onto conveyor belts. In other cases, transfer chutes are employed to direct the flow of bulk material from one conveyor belt to another, often via a three dimensional path. The importance of correct chute design to ensure efficient transfer of bulk solids without spillage and blockages and with minimum chute and belt wear cannot be too strongly emphasised. The importance is accentuated with the trend towards higher conveying speeds.

The paper describes how the relevant flow properties of bulk solids are measured and applied to chute design. Chute flow patterns are described and the application of chute flow dynamics to the determination of the most appropriate chute profiles to achieve optimum flow is illustrated. The influence of the flow properties and chute flow dynamics in selecting the required geometry to minimise chute and belt wear at the feed point will be highlighted.

1. INTRODUCTION

Undoubtedly the most common application of chutes occurs in the feeding and transfer of bulk solids in belt conveying operations. The importance of correct chute design to ensure efficient transfer of bulk solids without spillage and blockages and with minimum chute and belt wear cannot be too strongly emphasised. These objectives are accentuated with the trend towards higher conveying speeds.

While the basic objectives of chute design are fairly obvious, the following points need to be noted:

- chute should be symmetrical in cross-section and located central to the belt in a manner which directs the solids onto the belt in the direction of belt travel
- in-line component of the solids velocity at the exit end of the chute should be matched, as far as possible, to the belt velocity. This is necessary in order to minimise the power required to accelerate the solids to the belt velocity, but more importantly to minimise abrasive wear of the belt
- normal component of the solids velocity at the exit end of the chute should be as low as possible in order to minimise impact damage of the belt as well as minimise spillage due to particle re-bounding
- slope of the chute must be sufficient to guarantee flow at the specified rate under all conditions and to prevent flow blockages due to material holding-up on the chute bottom or side walls. It is implicit in this objective that the chute must have a sufficient slope at exit to ensure flow which means that there is a normal velocity component which must be tolerated

- adequate precautions must be taken in the acceleration zone where solids feed onto the belt in order to minimise spillage. Often this will require the use of skirtplates
- in the case of fine powders or bulk solids containing a high percentage of fines attention needs to be given to design details which ensure that during feeding aeration which leads to flooding problems, is minimised. For this to be achieved, free- fall zones or zones of high acceleration in the chute configuration should be kept to a minimum.

Chute design has been the subject of considerable research, a selection of references being included at the end of this paper [1-29]. However, it is often the case that the influence of the flow properties of the bulk solid and the dynamics of the material flow are given too little attention. The purpose of this paper is to focus on these aspects, indicating the basic principles of chute design with particular regard to feeding and transfer in belt conveying operations.

2. BOUNDARY FRICTION, COHESION AND ADHESION

2.1 Boundary or Wall Yield Locus

For chute design, wall or boundary surface friction has the major influence. It has been shown that friction depends on the interaction between the relevant properties of the bulk solid and lining surface, with external factors such as loading condition and environmental parameters such as temperature and moisture having a significant influence.

The determination of wall or boundary friction is usually performed using the Jenike direct shear test as illustrated in Figure 1(a). The cell diameter is 95mm. The shear force S is measured under varying normal force V and the wall or boundary yield locus, S versus V , or more usually shear stress τ versus normal stress σ is plotted.

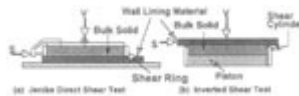


Figure 1. Boundary or Wall Friction Measurement

The Jenike test was originally established for hopper design for which the normal stresses or pressures are always compressive. In the case of chute design, the pressures are normally much lower than in hoppers, and often tensile, particularly where adhesion occurs due to the cohesive nature of the bulk solid. The Jenike test of Figure 1(a) does not allow low compressive pressures to be applied since there is always the weight of the bulk solid in the shear cell, the shear ring and lid which forms part of the normal load. To overcome this shortcoming, the inverted shear tester of Figure 1(b) was developed at the University of Newcastle. The shear cylinder is retracted so as to maintain contact between the bulk solid and the sample of the lining material. In this way, it is possible to measure the shear stress under low compressive and even tensile stresses. The inverted shear cell has been manufactured with a diameter of 300mm in order to allow more representative size distributions of bulk solids to be tested.

The boundary or wall yield loci (WYL) for most bulk solids and lining materials tend to be slightly convex upward in shape and, as usually is the case, each WYL intersects the wall shear stress axis indicating cohesion and adhesion characteristics. This characteristic is reproduced in Figure 2. The wall or boundary friction angle ϕ is defined by:

$$\phi = \tan^{-1} \left[\frac{\tau_w}{\sigma_w} \right] \quad (1)$$

where τ_w = shear stress at the wall; σ_w = pressure acting normal to the wall

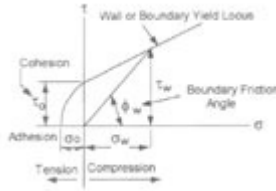


Figure 2. Wall or Boundary Friction and Adhesion Characteristics

The WYL for cohesive bulk solids is often convex upward in shape and, when extrapolated, intersects the shear stress axis at τ_0 . The Wall Friction Angle, ϕ , will then decrease with increase in normal pressure. This is illustrated in Figure 3 which shows the wall friction angles for a representative cohesive coal in contact with a dull and polished mild steel surfaces. It is to be noted that the wall friction angle cannot be larger than the effective angle of internal friction δ which is an upper bound limit for ϕ . Thus, for very low normal pressures where the friction angle ϕ can be quite large, the bulk solid will fail by internal shear rather than by boundary shear, leaving a layer of material on the surface.

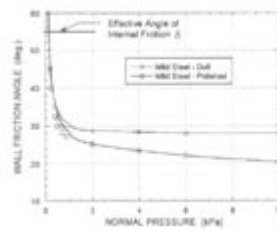


Figure 3. Friction Angles for a Particular Coal on Mild Steel Surfaces

The nature of adhesion and cohesion is quite complex; a study of this subject would require a detailed understanding of the physics and chemistry of bulk solid and surface contact. It is known, for example, that cohesion and adhesion generally increase as the wall surface becomes smoother relative to the mean particle size of the adjacent bulk solid. Also adhesion and cohesion generally increase as moisture content of the bulk solid increase, particularly in the case of very smooth surfaces. No doubt, in such cases, surface tension has a significant influence. Cohesion and adhesion can cause serious flow blockage problems when corrosive bonding occurs, such as when moist coal is in contact with carbon steel surfaces. The bonding action can occur after relatively short contact times. Impurities such as clay can also seriously aggravate the behavior due to adhesion and cohesion.

2.2 Types of Adhesion Problems

In order that build-up and hence blockages can be avoided, it is necessary for the body forces generated in the bulk mass to be sufficient to overcome the forces due to adhesion and shear. Figure 4 illustrates the types of build-up that can occur.

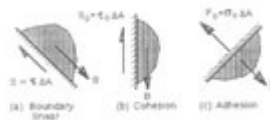


Figure 4. Build-Up on Surfaces
 S = Shear Force; B = Body Force; F_o = Adhesive Force

The body forces are normally those due to the weight component of the bulk solid but may also include inertia forces in dynamic systems such as in the case of belt conveyor discharge or, in other cases, when vibrations are applied as a flow promotion aid.

2.3 Mechanisms of Failure

When the body forces are sufficient to cause failure and, hence, flow, the mode of failure will depend on the relative strength versus shear conditions existing at the boundary surface and internally within the bulk solid. As discussed by Scott [29], the following failure conditions are considered:

(a) Failure Envelopes - General Case

In this case the shear stress versus normal stress failure envelope for a cohesive bulk solid is always greater than the failure envelope at the boundary. This is illustrated in Figure 5. For such cases, it is expected that failure will occur at the boundary surface rather than internally within the bulk solid.

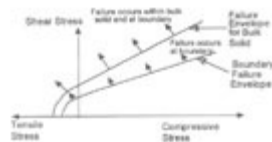


Figure 5 Failure Envelopes - General Case

(b) Failure Envelopes - Special Case

In cases of high moisture content cohesive bulk solids it is possible for the failure envelope of the bulk solid at lower consolidation stresses or pressures to give lower internal strength than the corresponding strength conditions at the boundary. This is depicted in Figure 6.5. The body forces may then cause failure by internal shear leaving a layer of build solid adhering to the chute surface. This layer may then build up progressively over a period of time.

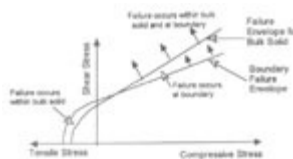


Figure 6. Failure Envelopes - Special Case

Often such problems arise in cases where the bulk solid is transported on belt conveyors leading to segregation with the fines and moisture migrating to the belt surface as the belt moves across the idlers. The segregation condition may then be transferred to chute surfaces. Other cases occur when the very cohesive carry-back material from conveyor belts is transferred to chute surfaces.

(c) Failure Envelope - Free Flowing Bulk Solids.

For free flowing, dry bulk solids with no cohesion, the boundary surface failure envelope is higher than the bulk solid failure envelope. In this case, adhesion of the bulk solid to a chute surface will not occur. Figure 6.6 illustrates this condition.

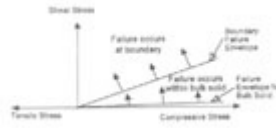


Figure 7. Failure Envelopes - Free Flowing Bulk Solids

The foregoing cases indicate that for failure and, hence, flow to occur, the shear stress versus normal stress state within the bulk solid near the boundary must lie above the failure envelope.

2.4 Example

Consider the case of a cohesive coal of bulk density $\rho = 1 \text{ t/m}^3$ which has a measured adhesive stress of $\sigma_0 = 1 \text{ kPa}$ for contact with mild steel, a typical value. The coal is attached to the underside of mild steel surface as illustrated in Figure 8. A vibrator is proposed as a means of removing the coal. Assuming a failure condition as depicted by Figure 5, the stable build up, denoted by the h_b , is given by

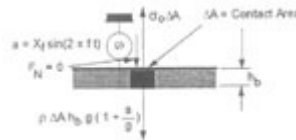


Figure 8. Adhesion Problem

$$h_b = \frac{\sigma_0}{\rho g \left(1 + \frac{a}{g}\right)} \quad (2)$$

where $a = (2 \pi f)^2 X_f$ = amplitude of applied acceleration

Without vibration (that is $a = 0$), $h_b = 0.1 \text{ m} = 100 \text{ mm}$, a substantial amount. To reduce h_b to say 10mm, an acceleration $a = 9.2 \text{ g}$ is required. There are many combinations of frequency and amplitude to achieve this. For instance, a frequency of $f = 151 \text{ Hz}$ and amplitude of $X = 0.1 \text{ mm}$ would suffice. This example indicates the difficulty of overcoming adhesion problems.

3. FEEDING OR LOADING CONVEYOR BELTS

Figure 9 illustrates the application of a gravity feed chute to direct the discharge from a belt or apron feeder to a conveyor belt. The bulk solid is assumed to fall vertically through a height 'h' before making contact with the curved section of the feed chute. Since, normally, the belt or apron speed $v_f \leq 0.5 \text{ m/s}$, the velocity of impact v_i with the curved section of the feed chute will be, essentially, in the vertical direction.

As a comment, the alternative to the use of an accelerating chute is to employ a short accelerating conveyor. These are high maintenance devices and still require head room. Feed chutes may be regarded as the better proposition.

3.1 Free Fall of Bulk Solid

For the free fall section, the velocity v_i may be estimated from

$$v_i = \sqrt{v_{fo}^2 + 2 g h} \quad (3)$$

Equation (3) neglects air resistance, which in the case of a chute, is likely to be small. If air resistance is taken into account, the relationship between height of drop and velocity V_i (Figure 9) is,

$$h = \frac{v_\infty^2}{g} \log_e \left[\frac{1 - \frac{v_{fo}}{v_\infty}}{1 - \frac{v_i}{v_\infty}} \right] - \left(\frac{v_{fo} - v_i}{g} \right) v_\infty \quad (4)$$

where v_∞ = terminal velocity

v_{fo} = vertical component of velocity of bulk solid discharging from feeder

V_i = velocity corresponding to drop height 'h' at point of impact with chute.

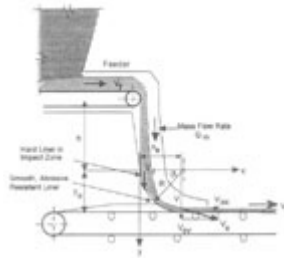


Figure 9. Feed Chute Configuration

3.2 Flow of Bulk Solid around Curved Chute of Constant Radius

The case of 'fast' flow around curved chutes is depicted by the chute flow model of Figure 10. The relevant details are

The drag force F_D is due to Coulomb friction, that is

$$F_D = \mu_E N \quad (5)$$

where μ_E = equivalent friction which takes into account the friction coefficient between the bulk solid and the chute surface, the stream cross-section and the internal shear of the bulk solid. μ_E is approximated by

$$\mu_E = \mu [1 + K_v H/B] \quad (6)$$

where μ = actual friction coefficient for bulk solid in contact with chute surface

K_v = pressure ratio. Normally $K_v \approx 0.4$ to 0.8 .

H = depth of flowing stream at a particular location
 B = width of chute

For continuity of flow,

$$\rho A v = \text{Constant} \quad (7)$$

where ρ = bulk density

A = cross-sectional area of flowing stream

It follows, therefore, that equation (6) can also be written as

$$\mu_E = \mu \left[1 + \frac{C_1}{v} \right] \quad (8)$$

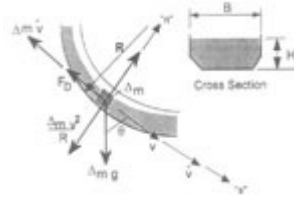


Figure 10. Chute Flow Model

For a chute of rectangular cross-section

$$C_1 = \frac{K_v v_o H_o}{B} \quad (9)$$

where v_o = initial velocity at entry to chute

H_o = initial stream thickness

Analysing the dynamic equilibrium conditions of Figure 10 leads to the following differential equation:

$$\frac{dv}{d\theta} + \mu_E v = \frac{gR}{v} (\cos \theta - \mu_E \sin \theta) \quad (10)$$

If the curved section of the chute is of constant radius R and μ_E is assumed constant at an average value for the stream, it may be shown that the solution of equation (10) leads to the equation below for the velocity at any location θ .

$$v = \sqrt{\frac{2gR}{4\mu_E^2 + 1} [(1 - 2\mu_E^2) \sin \theta + 3\mu_E \cos \theta] + K e^{-2\mu_E \theta}} \quad (11)$$

For $v = v_o$ at $\theta = \theta_o$,

$$K = \left\{ v_o^2 - \frac{2gR}{4\mu_E^2 + 1} [(1 - 2\mu_E^2) \sin \theta_o + 3\mu_E \cos \theta_o] \right\} e^{2\mu_E \theta_o} \quad (12)$$

$$4 \mu_E^2 + 1$$

Special Case:

$$\text{When } \theta_0 = 0 \text{ and } v = v_0, K = v_0^2 - \frac{6 \mu_E g R}{1 + 4 \mu_E^2} \quad (13)$$

Equation (11) becomes,

$$v = \sqrt{\frac{2 g R}{4 \mu_E^2 + 1} [(1 - 2 \mu_E^2) \sin \theta + 3 \mu_E \cos \theta] + K e^{-2\mu_E \theta} [v_i^2 - \frac{6 \mu_E R g}{4 \mu_E^2 + 1}]} \quad (14)$$

4 TRANSFER CHUTES

The foregoing discussion has focused on curved chutes of concave upward form in which contact between the bulk solid and the chute surface is always assured by gravity plus centrifugal inertia forces. In the case of conveyor transfers, it is common to employ chutes of multiple geometrical sections in which the zone of first contact and flow is an inverted curve. This is illustrated in Figure 11 in which the use of curved impact plates is employed in a conveyor transfer. The lining is divided into two zones, one for the impact region under low impact angles, and the other for the streamlined flow. The concept of removable impact plates, used in conjunction with spares allows ready maintenance of the liners to be carried out without interrupting the production.

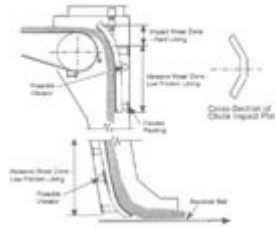


Figure 11. Transfer Chute Showing Impact Plates

4.1 Inverted Curved Chute Sections

The method outlined in Section 3.2 for curved chutes may be readily adapted to inverted curved chute section as illustrated in Figure 12. Noting that $F_D = \mu_E N$, it may be shown that the differential equation is given by

$$- \frac{dv}{d\theta} + \mu_E v = \frac{g R}{v} (\cos \theta + \mu_E \sin \theta) \quad (15)$$

For a constant radius and assuming μ_E is constant at an average value for the stream, the solution of equation (15) is

$$v = \sqrt{\frac{2 g R}{4 \mu_E^2 + 1} [\sin \theta (2 \mu_E^2 - 1) + 3 \mu_E \cos \theta] + K e^{2\mu_E \theta}} \quad (14)$$

For $v = v_0$ at $\theta = \theta_0$, then

$$K = \left\{ v_0^2 - \frac{2 g R}{1 + 4 \mu_E^2} [3 \cos \theta_0 + (2 \mu_E^2 - 1) \sin \theta_0] \right\} e^{-2\mu_E \theta_0} \quad (17)$$

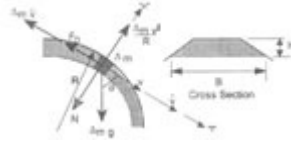


Figure 12. Inverted Curved Chute Model

Special Case: $v = v_0$ at $\theta_0 = \pi/2$

$$K = \left\{ v_0^2 - \frac{2 g R}{1 + 4 \mu_E^2} [2 \mu_E^2 - 1] \right\} e^{-\mu_E \pi} \quad (18)$$

and

$$v = \sqrt{ \frac{2 g R}{4 \mu_E^2 + 1} [\sin \theta (2 \mu_E^2 - 1) + 3 \mu_E \cos \theta] + e^{-\mu_E (\pi - 2\theta)} \left[v_0^2 - \frac{2 R g (2 \mu_E^2 + 1)}{4 \mu_E^2 + 1} \right] } \quad (19)$$

Equations (16) to (19) apply during positive contact, that is, when

$$\frac{v^2}{R g} \geq \sin \theta \quad (20)$$

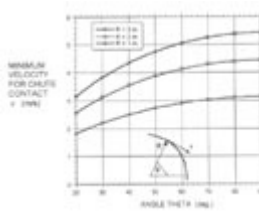


Figure 13. Minimum Velocities for Impact Chute Contact

The minimum bulk solid velocities for chute contact as a function of contact angle for three curve radii are presented in Figure 13.

4.2 Convex Chute Sections

On some occasions, it may be desirable to incorporate a convex curve as illustrated in Figure 14 in order to reduce the adhesion effects and assist the discharge process.

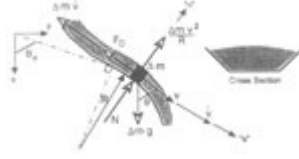


Figure 14. Convex Curved Chute Section

For $F_D = \mu_E N$, it may be shown that the differential equation is given by

$$\frac{dv}{d\theta} - \mu_E v = \frac{gR}{v} (\cos\theta - \mu_E \sin\theta) \quad (21)$$

This holds for

$$\sin\theta \geq \frac{v^2}{Rg} \quad (22)$$

It is noted that Figure 13 also applies in this case with the vertical axis now representing the maximum value of the velocity for chute contact.

For a constant radius and assuming μ_E is constant at an average value for the stream, the solution of equation (21) is

$$v = \sqrt{\frac{2gR}{4\mu_E^2 + 1} [(1 + 2\mu_E^2)\sin\theta - \mu_E \cos\theta] + K e^{2\mu_E \theta}} \quad (23)$$

For $v = v_0$ at $\theta = \theta_0$, then

$$K = \left\{ v_0^2 - \frac{2gR}{1 + 4\mu_E^2} [(1 + 2\mu_E^2)\sin\theta_0 - \mu_E \cos\theta_0] \right\} e^{-2\mu_E \theta_0} \quad (24)$$

Special Case: $v = v_0$ at $\theta_0 = \pi/2$

$$K = \left\{ v_0^2 - \frac{2gR}{1 + 4\mu_E^2} [1 + 2\mu_E^2] \right\} e^{-\mu_E \pi} \quad (25)$$

and

$$v = \sqrt{\frac{2gR}{4\mu_E^2 + 1} [(1 + 2\mu_E^2)\sin\theta + \mu_E \cos\theta] + e^{\mu_E (2\theta - \pi)} \left[v_0^2 - \frac{2Rg}{4\mu_E^2 + 1} \right]} \quad (26)$$

5. WEAR IN CHUTES

Chute wear is a combination of abrasive and impact wear. Abrasive wear may be analysed by considering the mechanics of chute flow as will be now described.

5.1 Abrasive Wear Factor of Chutes

In cases where the bulk solid moves as a continuous stream under 'fast' flow conditions the abrasive or rubbing wear may be determined as follows:

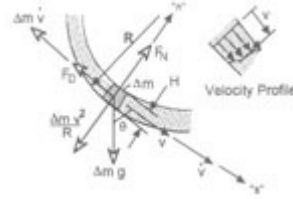


Figure 15. Chute Flow Model

(a) Wear of Chute Bottom

Consider the general case of a curved chute as shown in Figure 15, the chute being of rectangular cross-section. An abrasive wear factor W_c expressing the rate of rubbing against the chute bottom has been derived as follows:

$$W_c = \frac{Q_m g K_c \tan \theta}{B} N_{WR} \quad (27)$$

W_c has units of N/ms

N_{WR} is the non-dimensional abrasive wear number and is given by,

$$N_{WR} = \frac{v^2}{R g} + \sin \theta \quad (28)$$

The various parameters are

- θ = chute friction angle
- B = chute width (m)
- K_c = ratio v_s/v
- v_s = velocity of sliding against chute surface
- Q_m = throughput kg/s
- R = radius of curvature of the chute (m)
- v = average velocity at section considered (m/s)
- θ = chute slope angle measured from the vertical

The factor $K_c < 1$. For 'fast' or accelerated thin stream flow, $K_c \sim 0.6$. As the stream thickness increases K_c will reduce. Two particular chute geometries are of practical interest, straight inclined chutes and constant radius curved chutes.

(i) Straight Inclined chutes

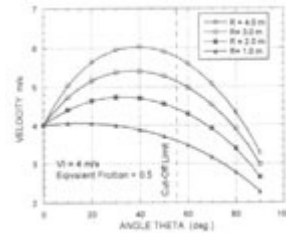
In this case $R = \infty$ and equation (27) reduces to

$$W_c = \frac{Q_m K_c \tan \theta g \sin \theta}{B} \quad (29)$$

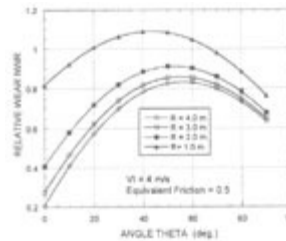
On the assumption that K_c is nominally constant, then the wear is constant along the chute and independent of the velocity variation.

(ii) Constant Radius Curved Chutes

In this case R is constant and the wear W_c is given by equations (27) and (28).



(a) Velocity Variation



(b) Abrasive Wear

Figure 16. Velocities and Wear in Chutes of Constant Curvature $Q=30 \text{ t/h}$; $v_o = 0.2\text{m/s}$; $\rho = 1 \text{ t/m}^3$; $b=0.5\text{m}$; $\mu_E = 0.6$; $\phi = 30^\circ$

The velocity variation around a constant radius curved chute is given by equations (11-14). By way of example, Figure 16(a) shows the variation of velocity, and Figure 16(b) the corresponding abrasive wear number as functions of angular position for constant curvature chutes of radii 1m, 2 m, 3 m and 4 m. It is interesting to observe that as R increases, the increase in N_{WR} becomes progressively smaller. In Figure 16(a), the limiting cut-off angle for the chutes to be self cleaning is indicated.

(b) Chute Side Walls

It is to be noted that the wear plotted in Figure 16 applies to the chute bottom surface. For the side walls, the wear will be much less, varying from zero at the stream surface to a maximum at the chute bottom. Assuming the side wall pressure to increase linearly from zero at the stream surface to a maximum value at the bottom, then the average wear on the side walls can be estimated from

$$W_{\text{CSW}} = \frac{W_c K_v}{2 K_c} \quad (30)$$

K_c and K_v are as previously defined. If, for example, $K_c = 0.8$ and $K_v = 0.4$, then the average side wall wear is 25% of the chute bottom surface wear.

5.2 Impact Wear in Chutes

Impact wear may occur at points of entry or points of sudden change in direction. For ductile materials, greatest wear is caused when impingement angles are low, that is in the order of 15° to 30°. For hard brittle materials, greatest impact damage occurs at steep impingement angles, that is angles in the vicinity of 90°.

6. WEAR OF BELT AT FEED POINT

An important application of feed and transfer chutes is to direct the flow of bulk solids onto belt conveyors. The problem is illustrated in Figure 17.

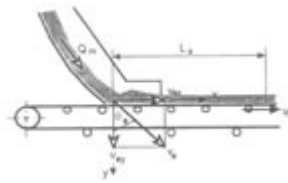


Figure 17 Feeding a Conveyor Belt

The primary objectives are to

- match the horizontal component of the exit velocity v_{ex} as close as possible to the belt speed
- reduce the vertical component of the exit velocity v_{ey} so that abrasive wear due to impact may be kept within acceptable limits
- load the belt centrally so that the load is evenly distributed in order to avoid belt mistracking
- ensure streamlined flow without spillage or blockages

6.1 Abrasive Wear Parameter

An abrasive wear parameter expressing the rate of wear for the belt may be established as follows:

$$\text{Impact pressure } p_{vi} = \rho v_{ey}^2 \quad (\text{kPa}) \quad (31)$$

where ρ = bulk density, t/m^3 ; v_{ey} = vertical component of the exit velocity, m/s

Abrasive wear parameter

$$W_a = \mu_b \rho v_{ey}^2 (v_b - v_{ex}) \quad (\text{kPa m/s}) \quad (32)$$

Where μ_b = friction coefficient between the bulk solid and conveyor belt; v_b = belt speed

The wear will be distributed over the acceleration length L_a .

Equation (32) may be also expressed as

$$W_a = \mu_b \rho v_e^3 K_b \quad (33)$$

$$\text{where } K_b = \cos^2\theta_e (v_b/v_e - \sin\theta_e) \quad (34)$$

θ_e = chute slope angle with respect to vertical at exit

K_b is a non-dimensional wear parameter. It is plotted in Figure 18 for a range of v_e/v_b values.

As indicated, the wear is quite severe at low chute angles but reduces significantly as the angle θ_e increases.

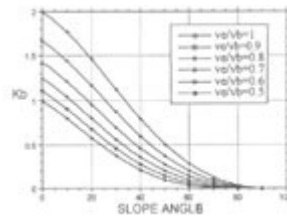


Figure 18. Non-Dimensional Wear Parameter versus Slope Angle θ

For the chute to be self cleaning, the slope angle of the chute at exit must be greater than the angle of repose of the bulk solid on the chute surface. It is recommend that

$$\alpha \geq \tan^{-1} (\mu_E) + 5^\circ \quad (35)$$

6.2 Acceleration Length

The acceleration length L_a over which slip occurs is given by

$$L_a = \frac{v_b^2 - v_{ey}^2}{2g m_b} \quad (36)$$

7. WEAR MEASUREMENT

The abrasive wear of chute lining and conveyor belt samples may be determined using the wear test apparatus illustrated in Figure 19.

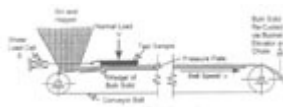


Figure 19. Wear Test Apparatus

As illustrated, the rig incorporates a surge bin to contain the bulk material, which feeds onto a belt conveyor. The belt delivers a continuous supply of the bulk material at a required velocity to the sample of material to be tested, which is held in position by a retaining bracket secured to load cells that monitor the shear load. The bulk material is drawn under the sample to a depth of several millimetres by the wedge action of the inclined belt. The required normal load is applied by weights on top of the sample holding bracket. The bulk material is cycled back to the surge bin via a bucket elevator and chute. The apparatus is left to run for extended periods interrupted at intervals to allow measurement of the test sample's weight and surface roughness if required. The measured weight loss is then converted to loss in thickness using the relationship given in equation (37).

$$\text{Thickness Loss} = \frac{M \cdot 10^3}{A \rho} \text{ mm} \quad (37)$$

where M = Mass loss (g)
 A = Contact Surface Area (m²)
 ρ = Test Sample Density (kg/m³)

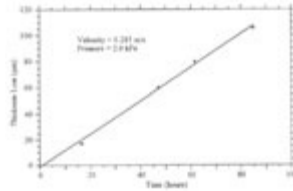


Figure 20. Wear Test Results

Tests have been conducted on samples of solid woven PVC conveyor belt using black coal as the abrading agent. A typical test result for a normal pressure of 2 kPa and a velocity of 0.285 m/s is given in Figure 20. The graph indicates a wear rate of approximately 1.3 μm/hour. This information may be used to estimate the wear expected to take place due to loading of coal on this type of conveyor belt.

8. CONVEYOR BELT DISCHARGE CHARACTERISTICS

8.1 General Discussion

Figure 21 shows the transition of a conveyor belt which may cause some initial lift of the bulk solid prior to discharge. The bulk solid will also have the tendency to spread laterally as the belt troughing angle decreases through the transition. The amount of spreading is more pronounced for free flowing bulk solids than for cohesive bulk solids. The spreading is also more pronounced at lower belt speeds. Once the bulk solid on the belt reaches the drum, a velocity profile may develop as illustrated in Figure 22. As a result of the velocity profile there will be a spread in the discharge trajectories

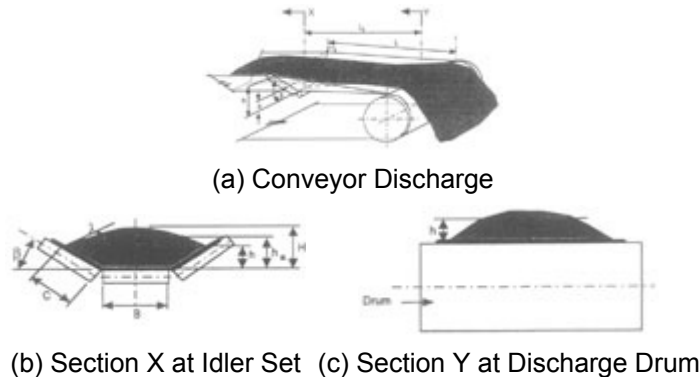


Figure 21. Conveyor Belt Transition Geometry and Load Profiles

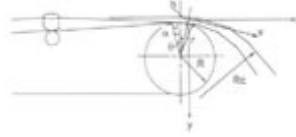


Figure 22 Belt Conveyor Transition

There will also be a variation in the adhesive stress across the depth of the stream. In most cases, however, the segregation that occurs during the conveying process will result in the moisture and fines migrating to the belt surface to form a thin boundary layer at the surface. This layer will exhibit higher adhesive stresses than will occur for the remainder of the discharging bulk solids stream. The magnitude of the adhesive stresses at the interface of the boundary layer and the belt surface will determine the extent of the carry-back on the belt

8.2 Profile of Bulk Solid on Belt

The conveyor throughput is given by

$$Q_m = \rho A v_b \quad (38)$$

Referring to Figure 21(b), the cross-sectional area at Section X is given by

$$A = U b^2 \quad (39)$$

where U = non-dimensional cross-sectional area factor
 b = contact perimeter

Assuming a parabolic surcharge profile, for a three-roll idler set, the cross-sectional area factor is given by

$$U = \frac{1}{(1 + 2r)^2} \left\{ r \sin \beta + \frac{r^2}{2} \sin 2\beta + \frac{\tan \lambda}{6} [1 + 4r \cos \beta + 2r^2 (1 + \cos 2\beta)] \right\} \quad (40)$$

where $r = C/B$ β = troughing angle λ = surcharge angle

8.3 Height of Bulk Solid on Belt at Idlers

a. Overall Height H (Figure 21(b))

$$H = C \sin \beta + (B + 2C \cos \beta) \frac{\tan \lambda}{4} \quad (41)$$

b. Mean height h_a

$$h_a = C \sin \beta + (B + 2C \cos \beta) \frac{\tan \lambda}{6} \quad (42)$$

8.4 Cross-Sectional Profile at Drive Drum

The profile shape at the drive drum, Figure 21(c), is difficult to determine precisely. It depends on the conveyor speed, cohesive strength of the bulk solid and the troughing configuration. The mean height h may be assumed to be

$$h = \frac{A}{(B + C)} \quad (43)$$

where A = cross-sectional area determined from equation (39).

8.5 Angle at which Discharge Commences

In order that the conditions governing discharge may be considered, the model of Figure 23 is considered. In general, slip may occur before lift-off takes place. Hence, the acceleration \dot{v} and inertia force $\Delta m \dot{v}$ are included in the model, v being the relative velocity. However, it is unlikely that slip will be significant so it may be neglected.

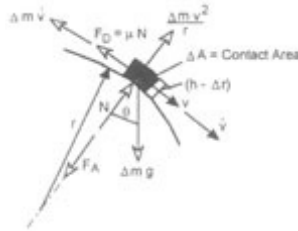


Figure 23 Conveyor Discharge Model

For an arbitrary radius r , the condition for discharge will commence when the normal force N becomes zero.

$$\frac{v^2}{r} = g \cos \theta + \frac{F_A}{\Delta m} \quad (44)$$

where $\Delta m = \rho \Delta A (h - \Delta r)$ = mass of element $F_A = \sigma_o \Delta A$ = adhesive force
 σ_o = adhesive stress ρ = bulk density

8.6 Minimum Belt Speed for Discharge at First Point of Drum Contact

In most cases, the speed of the conveyor is such that discharge will commence as soon as the belt makes contact with the discharge drum. In this case $\theta = -\alpha$, where α = slope of the belt at contact point with the drum. The critical case will be for the belt surface, that is, when $\Delta r = 0$. The minimum belt speed for discharge at the first point of drum contact is

$$v_b = \sqrt{R g \left(\cos \alpha + \frac{\sigma_o}{\rho g h} \right)} \quad (45)$$

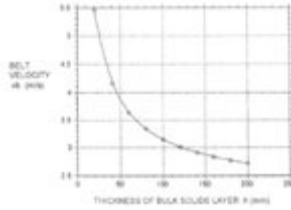


Figure 24 Belt Speed for Discharge at First Point of Drum Contact
 $R=0.5\text{m}$, $\rho=1\text{ t/m}^3$, $\alpha = 0^\circ$, $\sigma_o = 1\text{kPa}$.

Figure 24 illustrates the application of equation (45). The minimum belt velocity for discharge to occur at the first point of belt contact is plotted against bulk solids layer thickness 'h'. The graph applies to the case when $\alpha = 0^\circ$ and $\sigma_o = 1\text{ kPa}$. The need for higher belt speeds to achieve lift-off as the layer thickness decreases is highlighted. This indicates the difficulty of removing the thin layer of cohesive bulk solid that becomes the carry-back that is required to be removed by belt cleaners.

8.7 Discharge Trajectories

In most cases the influence of air drag is negligible. Hence the equations of motion simplify.

The equation of the path is

$$y = x \tan \theta + \frac{1}{2} g \frac{x^2}{v^2 \cos^2 \theta} \quad (46)$$

The bounds for the trajectories may be determined for the two radii $(R + h)$ and R for which the angle θ is obtained from equation (45).

9. CURVED IMPACT PLATES

Section 4.1 presented an analysis of flow around curved impact plates. Referring to Figure 22, the radius of curvature of the discharge trajectory is given by

$$R_c = \frac{[1 + (\frac{g x}{v_b^2 \cos^2 \theta})^2]^{1.5}}{\frac{g}{v_b^2 \cos^2 \theta}} \quad (47)$$

For contact to be made with a curved impact plate of constant radius, the radius of curvature of the trajectory at the point of contact must be such that,

$$R_c \geq R \quad (48)$$

where R_c = chute radius

Example

Consider the case of a conveyor discharge in which $v_b = 4 \text{ m/s}$, $\theta = 0^\circ$. The radius of curvature R_c as a function of horizontal distance 'x' is shown in Figure 25.

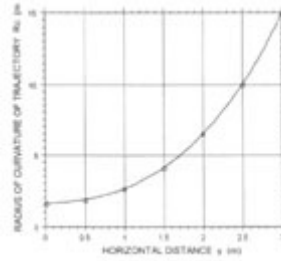


Figure 25. Radius of Curvature of Path $V_b = 4 \text{ m/s}$; $\theta = 0^\circ$

The curved impact plate may be positioned so that the chute radius matches the radius of curvature at the point of contact. This is illustrated in Figure 26.

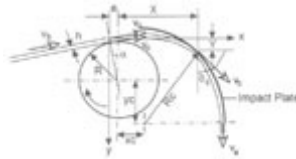


Figure 26. Impact Plate and Trajectory Geometry

10. CHUTES OF THREE DIMENSIONAL GEOMETRY

Although this paper has concentrated on chutes of two dimensional geometry, the concepts presented may be readily extended to the three dimensional case. Using the lumped parameter model approach, the equations of motion may be expressed in the most convenient co-ordinate system relevant to the particular chute profiles. The example of a transfer chute for the receiving conveyor at 90° to the delivering conveyor is summarised.

Problem Specification:

Bulk Material - Bauxite
 Bulk density as loaded $\rho = 1.3 \text{ t/m}^3$
 throughput $Q_m = 2500 \text{ t/h}$
 Belt speed, delivery belt $v_b = 5 \text{ m/s}$
 Belt speed, receiving belt, $v_b = 5 \text{ m/s}$;
 Surcharge angle of bauxite on belt $\lambda = 25^\circ$
 Conveyor inclination $\alpha = 10^\circ$
 Effective drive drum diameter = 1.2 m
 Idler inclination angle $\beta = 35^\circ$
 Receiving belt at right angle to delivery belt

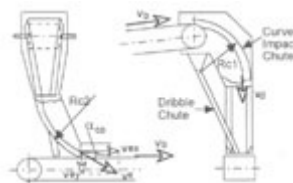


Figure 27. Transfer Chute Example

Referring to Figure 26 and 27, the design parameters are:

Impact Chute: $R_{c1} = 2.8\text{m}$; Contact angle $\theta_c = 74.2^\circ$; $v_c = 5.12\text{ m/s}$; $x_c = 0.238\text{m}$; $y_c = 1.96\text{m}$; $v_d = 6.75\text{m/s}$

Feed Chute: $R_{c2} = 3.0\text{m}$; $v_e = 5.57\text{ m/s}$ at cut off angle $\theta = 55^\circ$; $v_{ex} = 4.57\text{ m/s}$; $v_{ey} = 3.12\text{m/s}$;
Wear $W_a = 2.26\text{ kPa m/s}$

11. CONCLUDING REMARKS

An overview of chute design with special reference to belt conveying operations has been presented. Particular attention has been directed at the need to measure the relevant flow properties of the bulk solid and to integrate these properties into the chute design process. Chute flow patterns have been described and the application of chute flow dynamics to the determination of the most appropriate chute profiles to achieve optimum flow has been illustrated.

12. REFERENCES

1. CHARLTON, W. H., CHIARELLA, C. and ROBERTS, A. W., "Gravity Flow of Granular Materials in Chutes: Optimising Flow Properties". Jnl. Agric. Engng. Res., Vol. 20, 1975, pp. 39-45.
2. CHARLTON, W. H and ROBERTS, A. W., "Chute Profile for Maximum Exit Velocity in Gravity Flow of Granular Materials". Jnl. Agric. Engng. Res., Vol. 15, 1970.
3. CHARLTON, W. H. and ROBERTS, A. W., "Gravity Flow of Granular Materials: Analysis of Particle Transit Time". Paper No. 72, MH-33, A.S.M.E., (presented at 2nd Symposium of Storage and Flow of Solids, Chicago, U.S.A., September 1972)
4. CHIARELLA, C. and CHARLTON, W. H., "Chute Profile for Minimum Transit Time in the Gravity Flow of Granular Materials". Jnl. Agric. Engng. Res., Vol. 17, 1972.
5. CHIARELLA, C., CHARLTON, W. H. and ROBERTS, A. W., "Optimum Chute Profiles in Gravity Flow of Granular Materials: A Discrete Segment Solution Method": Paper No. 73, MH-A, A.S.M.E., 1972.
6. CHIARELLA, C., CHARLTON, W. H. and ROBERTS, A. W., "Gravity Flow of Granular Materials: Chute Profiles for Minimum Transit Time". Paper Presented at Symposium on 'Solids and Slurry Flow of and Handling in Chemical Process Industries', AIChE, 77th National Meeting, June 1974, Pittsburg, U.S.A.
7. Chute Design, First International Conference, Bionic Research Institute, Johannesburg, South Africa, 1991.
8. "Chute Design Problems and Causes", Seminar, Bionic Research Institute, Johannesburg, South Africa, February 1992.
9. LONIE, K.W., "The Design of Conveyor Transfer Chutes". Paper Reprints, 3rd Int Conf on Bulk Materials Storage, Handling and Transportation, Newcastle, NSW, Australia, June 1989, pp 240-244.

10. MARCUS, R.D., BALLER, W.J. and BARTHEL, P. "The Design and Operation of the Weber Chute". Bulk Solids Handling, Vol. 16, No.3, July/September 1996. (pp.405-409).
11. ROBERTS, A. W., "The Dynamics of Granular Materials Flow through Curved Chutes". Mechanical and Chemical Engineering Transactions, Institution of Engineers, Australia, Vol. MC3, No. 2, November 1967.
12. ROBERTS, A. W., "An Investigation of the Gravity Flow of Non-cohesive Granular Materials through Discharge Chutes". Transactions of A.S.M.E., Jnl. of Eng. in Industry, Vol. 91, Series B, No. 2, May 1969
13. ROBERTS, A.W., "Bulk Solids Handling : Recent Developments and Future Directions". Bulk Solids Handling, 11(1), 1991, pp 17-35.
14. ROBERTS, A.W., OOMS, M. and WICHE, S.J., "Concepts of Boundary Friction, Adhesion and Wear in Bulk Solids Handling Operations". Bulk Solids Handling, 10(2), 1990, pp 189-198.
15. ROBERTS, A.W., SCOTT, O.J. and PARBERY, R.D., "Gravity Flow of Bulk Solids through Transfer Chutes of Variable Profile and Cross-Sectional Geometry". Proc of Powder Technology Conference, Publ by Hemisphere Publ Corp, Washington, DC, 1984, pp 241-248.
16. ROBERTS, A.W. and CHARLTON, W.H., "Applications of Pseudo-Random Test Signals and Cross-Correlation to the Identification of Bulk Handling Plant Dynamic Characteristics". Transactions of A.S.M.E., Jnl. of Engng. for Industry, Vol. 95, Series B, No. 1, February 1973.
17. ROBERTS, A. W., CHIARELLA, C. and CHARLTON, W. H., "Optimisation and Identification of Flow of Bulk Granular Solids". Proceedings IFAC Symposium on Automatic Control in Mining, Mineral and Metal Processing, Inst. of Engrs., Aust., Sydney, 1973.
18. ROBERTS, A. W. and ARNOLD, P. C., "Discharge Chute Design for Free Flowing Granular Materials". Transactions of A.S.A.E., Vol. 14, No. 2, 1971.
19. ROBERTS, A. W. and SCOTT, O. J., "Flow of Bulk Solids through Transfer Chutes of Variable Geometry and Profile". Proceedings of Powder Europa 80 Conference, Wiesbaden, West Germany, January 1980.
20. ROBERTS, A. W. and MONTAGNER, G. J., "Identification of Transient Flow Characteristics of Granular Solids in a Hopper Discharge Chute System". Paper presented at Symposium on Solids and Slurry Flow and Handling in Chemical Process Industries, AIChE, 77th National Meeting, June 2-5, 1974, Pittsburg, Pa., U.S.A.
21. ROBERTS, A. W. and MONTAGNER, G. J., "Flow in a Hopper Discharge Chute System". Chem. Eng. Prog., Vol. 71, No.2, February 1975.
22. ROBERTS, A. W., SCOTT, O. J. and PARBERY, R. D., "Gravity Flow of Bulk Solids through Transfer Chutes of Variable Profile and Cross-Sectional Geometry". Proceedings of International Symposium on Powder Technology, Kyoto, Japan, September 1981.
23. ROBERTS, A. W. and SCOTT, O. J., "Flow of Bulk Solids through Transfer Chutes of Variable Geometry and Profile". Bulk Solids Handling, Vol. 1, No. 4, December 1981, pp. 715.

24. ROBERTS, A.W. "Basic Principles of Bulk Solids Storage, Flow and Handling", TUNRA Bulk Solids, The University of Newcastle, 1998.
25. ROBERTS, A.W. and WICHE, S.J. "Interrelation Between Feed Chute Geometry and Conveyor Belt Wear". Bulk Solids Handling, Vol. 19, NO.1 January, March 1999
26. ROBERTS, A.W. "Mechanics of Bucket Elevator Discharge During the Final Run-Out Phase". Intl. of Powder and Bulk Solids Technology, Vol. 12, No.2, 1988. (pp.19-26)
27. SAVAGE, S. B., "Gravity Flow of Cohesionless Granular Materials in Chutes and Channels". J. Fluid Mech. (1979), Vol. 92, Part 1, pp. 53-96.
28. SAVAGE, S.B., "The Mechanics of Rapid Granular Flows". Adv Appl Mech, 24, 1984, pp 289.
29. SCOTT, O.J., "Conveyor Transfer Chute Design, in Modern Concepts in Belt Conveying and Handling Bulk Solids". 1992 Edition. The Institute for Bulk Materials Handling Research, University of Newcastle, 1992, pp 11.11-11.13.